Tailoring low energy electron absorption *via* surface nano-engineering of cesiated chromium films

Andre L. Fernandes Cauduro,[1,a)] Lucas H. Hess,[2] D. Frank Ogletree,[3] Jared W. Schwede, [2,4] and Andreas K. Schmid[1,a)]

[1] *National Center for Electron Microscopy, Molecular Foundry, Lawrence Berkeley National Laboratory, Berkeley, California 94720, USA*

[2] *Spark Thermionics, Inc., Berkeley, California 94720, USA*

[3] *Molecular Foundry, Lawrence Berkeley National Laboratory, Berkeley, California 94720, USA*

[4] *Lawrence Berkeley National Laboratory, Berkeley, California 94720, USA*

a) Electronic mail: alcauduro@lbl.gov (A.L.F.C.); akschmid@lbl.gov (A.K.S.);

Abstract

In this letter we demonstrate that improved low energy electron absorption is achieved by suppressing the crystallinity of chromium thin-films grown on W[110], which points to a promising route for achieving highly-efficient thermionic energy converters (TECs). Using low energy electron microscopy (LEEM) and in-situ film growth, we show that substrate temperature control permits well-controlled fabrication of either epitaxial Cr[110] films or nano-crystalline Cr layers. We show that the work function of cesium saturated nano-crystalline Cr thin-films is ~0.20 eV lower than that of epitaxial Cr[110] films. Our LEEM measurements of absorbed and reflected currents as a function of electron energy demonstrate that nano-crystallinity of cesiated chromium films results in 96% electron absorption in the range of up to 1 eV above the work function, compared to just 79% absorption in cesiated crystalline Cr[110] films. These results point to metal films with suppressed crystallinity as an economical and scalable means to synthesize nano-engineered surfaces with optimized properties for next generation anode materials in high performance thermionic energy converters.

Thermionic energy converters (TECs) are heat engines, operating under vacuum, that directly convert heat to electrical power. The underlying physical mechanisms are well understood and are based on heating an electrode, typically a refractory material, to high temperature so that electrons gain enough thermal energy to overcome the vacuum barrier.[1] These electrons are then driven by a work function difference across a vacuum gap between the cathode and a low work function anode where they are collected to provide electrical power output. The electrons emitted from the hot cathode obey the Richardson-Dushmann equation ($J = AT^2 \exp(\frac{-\Phi}{kT})$), where A is the Richardson constant, k the Boltzmann constant, T the temperature and Φ (eV) the work function of the emitter.[2] As electrons are emitted into the vacuum gap, a significant space charge layer can be formed, which acts as potential barrier that lowers the output power and therefore the conversion efficiency of a given TEC. [3]

One key approach to mitigating space charge layer formation is decreasing the gap distance between the cathode and anode. Numerical results reported by Lee *et al.*[3] show that energy conversion efficiencies of 50% or more may be achievable in optimized micro-gapped TECs, and the construction of devices with such gap sizes is possible today *via* microfabrication. However, this approach may introduce new efficiency limitations such as parasitic heating losses associated to heat transfer through micro meter gaps. As recently discussed by Lim *et al.*,[4] controlling electron reflectivity at the collector surface is an under-appreciated element in mitigating space-charge losses. In addition to the importance of managing total reflectivity, they point out that non-specular reflection, such as diffuse scattering, contributes less space charge than specular reflection, as electrons fall off outside an escape cone formed upon reflection on the anode surface. Also, wide-angle reflection may increase the probability of

collection as electrons bounce on the anode's surface. [4,5] As predicted by Islam *et al.,*[5] the use of rough anodes may simultaneously reduce reflection and encourage diffuse scattering of low energy electrons impinging a surface. [5] In the work reported here, we combine low energy electron microscopy (LEEM) and current absorption measurements using LEEM together with low energy electron diffraction (LEED) under *in operando* conditions. We show that this experimental approach, essentially mimicking operating conditions of a TEC cell inside the LEEM, allows direct assessment of the key physical parameters of TEC electrode materials, including electron reflectivity and work function.

LEEM is a surface imaging technique that decelerates an electron beam to very low energy (0-50 eV) with a retarding field at the specimen's surface. Imaging elastically reflected electrons makes the method very sensitive to the chemical, physical, and structural properties of the first few atomic layers. [6,7] LEEM combines good spatial resolution (a few tens of nm in our instrument) with spectral information by recording the intensity of reflected electrons as function of their landing energy on the surface, namely *intensity-vs.-voltage* or *I-V* LEEM. Pixel-by-pixel evaluation of the electron reflectivity vs. landing energy produces high-resolution 2D work function maps. [8–10] Here we use this technique for measuring work function and for quantifying electron reflectivity of prototype anodes materials for thermionic energy converters, characterizing anode materials under *in operando* conditions, *i.e.*, including variable coverage cesium overlayers which are used in virtually all conventional thermionic devices.[1] We demonstrate that appropriate Cr thin-film growth temperatures promote the formation of a nano-crystalline Cr. After cesiation, this nano-crystallinity significantly reduces the electron reflectivity in the energy window relevant for TECs, increasing electron absorption by 33% over otherwise similar epitaxial Cr[110] thin-films. Our experiments show that not only is specular reflection

suppressed, but the effective cesiated work function is also reduced relative to epitaxial films.

The W[110] substrate crystal was cleaned by flash heating to ~2000°C every 5 min in $3x10^{-8}$ Torr of oxygen over a period of ~12h, to obtain a surface free of contaminations. The last flash was performed in UHV (~$1x10^{-10}$ Torr) to desorb the oxygen layer. Chromium films were prepared *in situ* by e-beam evaporation on the W[110] crystal inside the LEEM chamber at a base pressure of $1x10^{-10}$ Torr. The Cr deposition rate was calibrated by monitoring LEEM-reflectivity oscillations during the formation of the first two atomic monolayers (ML). Oscillations in backscattered electron current during deposition indicate atomic monolayer-by-monolayer growth.[11,12] This layer-by-layer growth mode is lost after the first few monolayers, so that continued deposition up to a total thickness equivalent to 20ML results in smooth films with a high degree of structural disorder, shown by the total absence of LEED spots. Single crystalline Cr[110] films were prepared by UHV annealing of the as-deposited Cr films at ~400°C for 40 s, following the recipe described in ref. [11]; LEED and LEEM were used to confirm single-crystallinity and atomic level smoothness of the resulting epitaxial Cr/W[110] films. Absorption current measurements were carried out using a Keithley 237 source-measure unit controlled by MATLAB code. Our W[110] crystal has a small thru-hole in the center to form a Faraday cup. The total beam current was monitored with high precision by periodically moving the crystal to collect the beam with the Faraday cup.

Fig. 1 shows LEEM and LEED images of typical samples as used in this study. Dark lines separating bright bands in fig. 1a indicate the step/terrace morphology of the well-ordered bulk-terminated W[110]. As seen in fig. 1b, after deposition of a Cr dose equivalent to 20ML onto the W[110] substrate at room temperature the step/terrace substrate morphology is essentially obscured, leaving only tall step-bunches visible under the rougher and nano-

granular surface morphology of the Cr film. LEED images of this type of Cr film (not shown) are completely diffuse and devoid of any reflexes, indicating a highly disordered, or nano-crystalline structure. In addition, extremely low specular electron reflectivity at all energies above the work function is another indication of the disordered structure of this film. Post-growth annealing at 400°C for 40s leads to crystallization of the Cr layer, forming an epitaxial single crystalline Cr[110]/W[110] film: the LEEM image and LEED pattern shown in fig. 1c and 1d, respectively, indicate smooth surface morphology and sharp LEED spots typical of a single crystalline film, similar to literature reports. [11–13]

To study the performance of epitaxial versus nano-crystalline Cr surfaces as TEC anodes, we turn our attention to the electron absorption/reflection properties of these surfaces after dosing Cs. The as-deposited nano-crystalline Cr films remain disordered after cesiation, and LEED images remained completely diffuse and devoid of any spots, while specular electron reflectivity remained extremely low at all energies above the work function. In contrast, cesiation of the Cr[110] surface leads to a LEED pattern indicating a well-ordered epitaxial overlayer with a supercell that is close to the (2x2) structure, albeit strained, expected from the Nishiyama-Wassermann epitaxial relationship. [14,15] Fig. 1e and 1f show a LEEM image and a LEED pattern, respectively, after ~ 1.5 ML cesium was deposited at room temperature on the single-crystalline Cr[110]/W[110] surface.

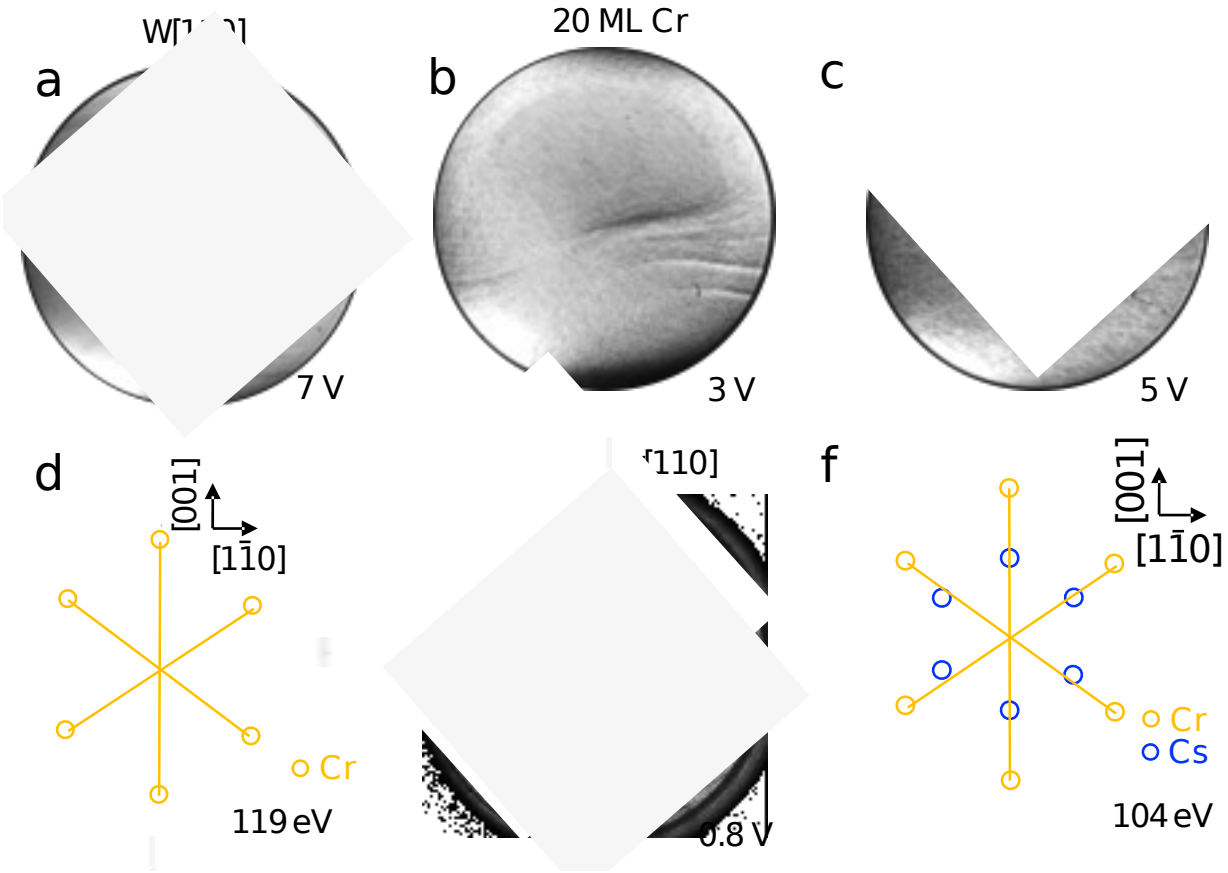

Fig. 1 – Bright-field LEEM images and LEED patterns of typical samples. a) BF-LEEM of W[110] at 7V landing energy. b) BF-LEEM at 3V of 20ML-equivalent nano-crystalline Cr grown at room temperature on W[110]. c) BF-LEEM at 5V of a post-growth annealed (400°C for 40s) 20ML Cr[110] film. d) LEED confirms the homoepitaxial structure of Cr[110] formed after post-annealing in UHV. e) BF-LEEM at 0.8V of cesiated Cr[110] film similar to the film of panels c, d. f) LEED confirms the Cs superstructure (blue circles) on Cr[110] (orange circles). BF-LEEM images were taken using a low objective extractor voltage (2kV), field of view is ~15 μm.

Electron reflectivity and work function are the two critical physical parameters for TEC anode performance, and these evolve as a function of Cs coverage (θ_{Cs}). In LEEM *I-V* spectra there is a well-defined steep reflectivity drop-off as the electron energy is increased above the work function of the sample, this intensity drop is used to track work function under in-situ anode preparation conditions. For consistent quantitative work function estimates, we determine V_S^0, the well-defined steep reflectivity drop-off, by fitting *I-V*

LEEM spectra with an error function (erfc) as detailed in fig. S1. The energy scale (horizontal axis) in all *I*-*V* LEEM plots in the main part of this paper includes the calibration offset by the work function of the cathode ($\phi_{Cathode}$ $1.4eV$). The data analysis procedures and energy scale calibration are further described in the supplementary materials (supplementary note #1 and fig.S1).

Fig. 2 summarizes *I*-*V* LEEM data that show how work function and reflectivity of two chromium surfaces, nano-crystalline Cr and epitaxial Cr[110], evolve as a function of Cs coverage. In panels a and b electron reflectivity is represented in a color scale, to permit plotting the evolution of reflectivity as a function of electron landing energy (horizontal axis) and cesium deposition time (vertical axis). Electron reflectivity across the full range from zero to 100% is represented in colors ranging from black to white, as shown in the color scale above panels a, b. Both cesiation experiments summarized in fig. 2 a-b show a similar trend in the work function evolution as a function of θ_{Cs}. Before the start of cesium deposition, marked by red solid lines in panels a and b, the work function of the nano-crystalline and single-crystalline Cr surfaces is around 4.5 eV and 5.0 eV, respectively. These values are in agreement with earlier works that reported the work function of polycrystalline Cr[16] and Cr[110]/W[110].[17] With cesium deposition at constant rate the work function decreases approximately linearly and a minimum value is reached (green dashed lines), finally the work function rises again and saturates for higher cesium coverage (blue solid lines) near the literature values for the work function of bulk cesium.[18] This type of work function dependence on coverage θ_{Cs} matches prior observations [19,20] and is well explained in the orbital-overlap model discussed by Chou *et al*., [21] where the initial approximately linear decrease is attributed to the linearly increasing density of individual, non-interacting, surface point dipoles (low coverage). A work function minimum is reached as the cesium

coverage increases and covalent interaction between the alkali adsorbates increases (intermediate coverage). Finally, the work function saturates at a value corresponding to the work function of bulk cesium. Detailed work function measurements are summarized in panels c and d. Here, *I-V* LEEM spectra are shown from un-cesiated, cesiated up to work function minimum, and cesium saturated surfaces are plotted in red, green, and blue curves, respectively (corresponding color-scale spectra are marked by red, green, and blue lines in panels a and b). Applying to these data the error-function fitting procedure as described in supplementary materials (figure S1) yields the work function values reported in the insets in panels b and c.

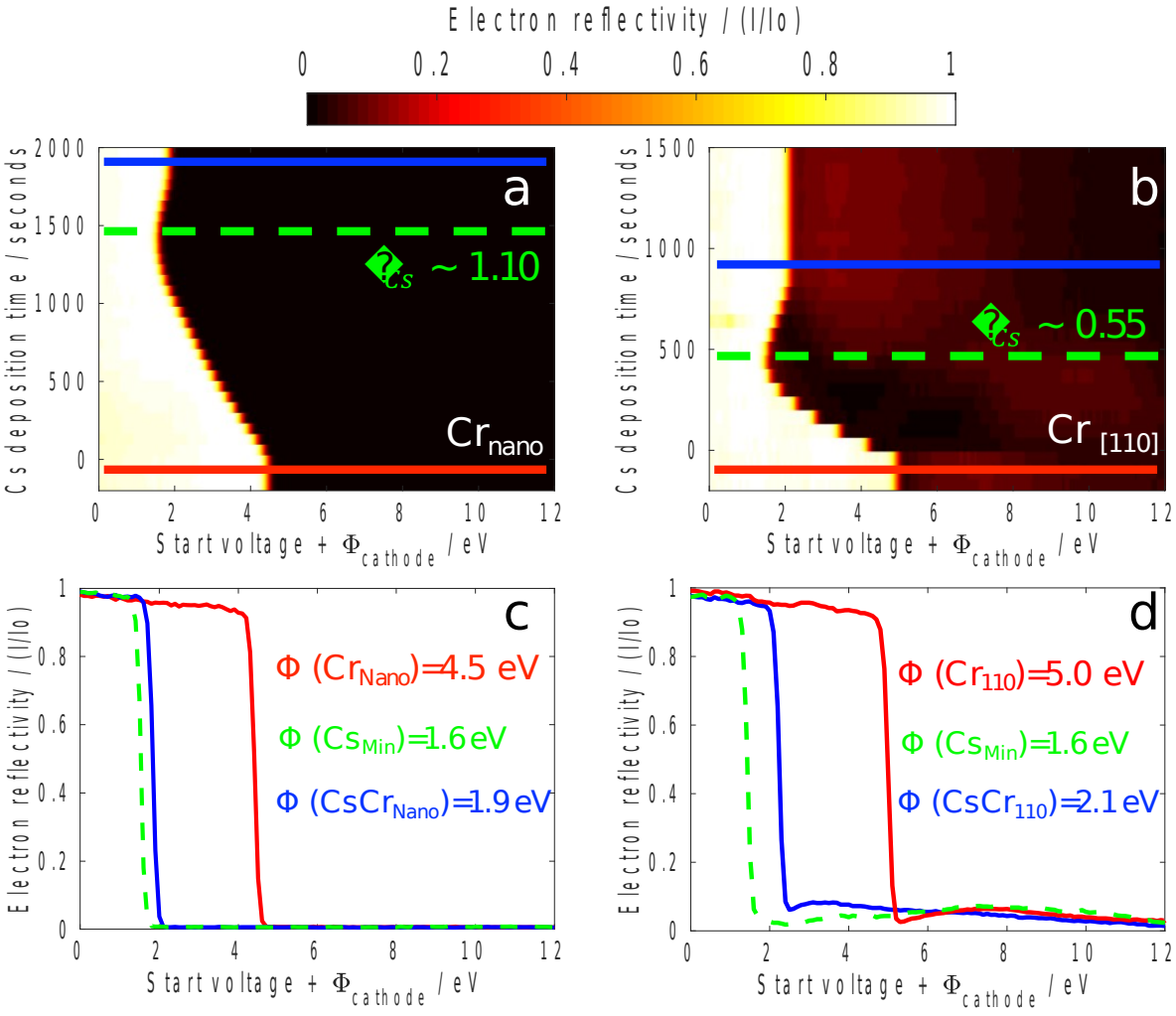

Fig. 2 – *I/V* LEEM spectra recorded as a function of Cs coverage. Panels a and b represent reflectivity in color according to scale above, plotted versus electron energy (horizontal axis) and Cs deposition time (vertical axis). a) cesiation of the

nano-crystalline chromium surface and b) of the Cr[110] surface. Three regions highlighted in panels a and b indicate: bare substrate (red line), minimum work function condition (dashed green line) and Cs saturated condition (blue line). In colors corresponding to the lines in a and b, panels c and d plot electron reflectivity as a function of start voltage (*I/V* curves) for several stages of cesium deposition on (c) nano-grained Cr films and (d) Cr[110] films. Insets in c and d indicate the work function values extracted by complementary error function (erfc) fitting of the intensity drop-off (for fitting procedure see supplementary materials). "Io" represents the intensity of reflected electrons in mirror mode (100% reflection).

In terms of minimal achieved work function under optimal cesium coverage, the performance potential for TEC applications of nano-crystalline Cr is similar to Cr[110]: in both structures the work function minimum is ~1.6eV. However, the nanocrystalline material is more robust since it maintains a lower work function in over-cesiated conditions: the nano-crystalline material saturates at a work function of ~1.9eV, which is 0.2 eV lower than the value of ~2.1eV seen in over-cesiated Cr[110]. The disordered crystalline structure of the saturated cesium films on nano-crystalline Cr is a plausible reason for the lower work function compared to saturated cesium on Cr[110]. Our LEED measurements reported above (fig. 1 and text) provide evidence towards this interpretation.

Our data reveal additional differences that have important implications for TEC device technologies. One, we observe that the alkali-coverage at which work function minima are reached is approximately 2.5 times larger in case of the nano-crystalline Cr surfaces, as compared to single-crystalline Cr[110] surfaces (see supplementary information, figures S2, S3), where minimum work function was associated with coverage θ_{Cs} 0.55 in ref.[21]. The surface of the nano-crystalline Cr layers is presumably far less densely packed than Cr[110]. Following the orbital-overlap model discussed by Chou *et al.*,[21] Cs atoms would interact much more with the less densely packed nano-crystalline substrate. As a result less Cs-Cs orbital overlap would occur, and thus more cesium is needed to achieve the coverage regime where point-dipoles start to become depolarized due to covalent interactions. [22] In order

to test if indeed the nano-crystalline surface has a higher Cs coverage in the work function minimum condition, we measured surface composition in both cases using Auger electron spectroscopy. The Auger spectrum of the cesiated minimum work function nano-crystalline Cr surface indicates approximately twice as much Cs than cesiated Cr[110] epi-layers (see supplementary information, fig. S3). These observations suggest that, compared to crystalline anodes, the nano-crystalline Cr layers may be more tolerant to variations in the Cs chemical potential under variable operation conditions of TEC devices. Another factor that may contribute to delay the work function minima is weaker Cs-Cs interaction due to higher surface area of the nano-crystalline Cr film in comparison to the atomically flat Cr[110], i.e., higher Cs dose is needed to induce covalent interactions.

An additional benefit of the nano-crystalline prototype anodes is suppression of electron reflectivity over an extended energy range. TEC anodes must collect electrons, so in operation the key electron energy range is a narrow window just above the work function. In panel d of fig. 2, the *I/V* LEEM spectra do not drop to zero in the energy range above the work function: evidently, in these cesiated crystalline Cr[110] films reflectivity remains significant, of the order of a few % up to about 10% in fig. 2d. The case of nano-crystalline Cr films is very different: in fig. 2c *I/V* LEEM reflectivity essentially vanishes at all energies above the work function, under all conditions of cesiation. 2D work function maps of Cr[110], cesiated Cr[110], nano-crystalline Cr, and cesiated nano-crystalline surfaces are displayed in supplementary material fig.S4-S7 and are discussed in more detail in supplementary note #3. This analysis shows that very slight work function variations of the order of <100mV are observed on the crystalline samples, and the nano-crystalline surface shows nearly featureless work function across its surface, with no workfunction “patches” nor significant lateral variations across the sample. Cesiated nano-crystalline Cr under saturation conditions exhibits work function variation of <50mV across 12μm field of

view. In the following section we discuss the suppression of electron reflectivity in more detail.

Due to design constraints of the LEEM instrument used here, the reflectivity measurements shown in figure 2 include only the specularly reflected current. Specular reflection is understood to contribute most severely to space charge induced TEC performance limitation,[4] but total reflected current, I_R, might also include off-specular or diffuse reflections that also contribute performance-degrading space-charge. In our LEEM the total reflected current cannot be measured directly. However, by measuring the total absorbed current, I_A, we can measure the total reflected current by accounting for charge conservation, i.e. total reflection and total absorption must add up to the total beam current I_B that is incident on the sample. To enable precise monitoring of beam current and absorbed current, a customized W[110] crystal with a pinhole was developed. The sample current can be measured either with the W[110] crystal exposed to the electron beam, which results in a measurement of I_A, or this sample was used as a Faraday cup by placing it into a position so that the electron beam is absorbed through the pinhole, which results in a measurement of I_B. This allows us to deduce the value of the total reflected current as $I_R = I_B - I_A$ with good accuracy. Fig. 3 shows quantitative measurements of the total electron reflection, as a function of electron landing energy.

Fig. 3a shows the current absorbed on the as-deposited and nano-crystalline Cr film (red solid curve) and after surface cesiation (blue solid curve). In addition, the black curves labeled FC1 and FC2 are Faraday cup measurements of the total beam current, acquired by absorbing the beam through the pinhole in the W[110] substrate. The curve FC1 was measured before cesiation and FC2 was re-measured after the cesiation, essentially identical results confirm that the beam current in the microscope is stable over time. Similarly, fig. 3b shows the absorbed current on the bare Cr[110]

surface (red solid line) and after surface cesiation (blue solid curve) and, again, LEEM beam current measured before and after cesiation, FC1 and FC2 (in black solid lines). To estimate the performance potential of these prototype cathodes in TEC device applications we can compare absorbed current in the most relevant landing energy range extending from work function up to ~1 eV above. As indicated by shaded regions, we find that around 96% of the incoming electrons are absorbed in the cesiated nano-crystalline Cr, while only about 79% of the beam is absorbed in cesiated Cr[110] surfaces. A full description of the analysis can be found in fig. S8 and supplementary note #4.

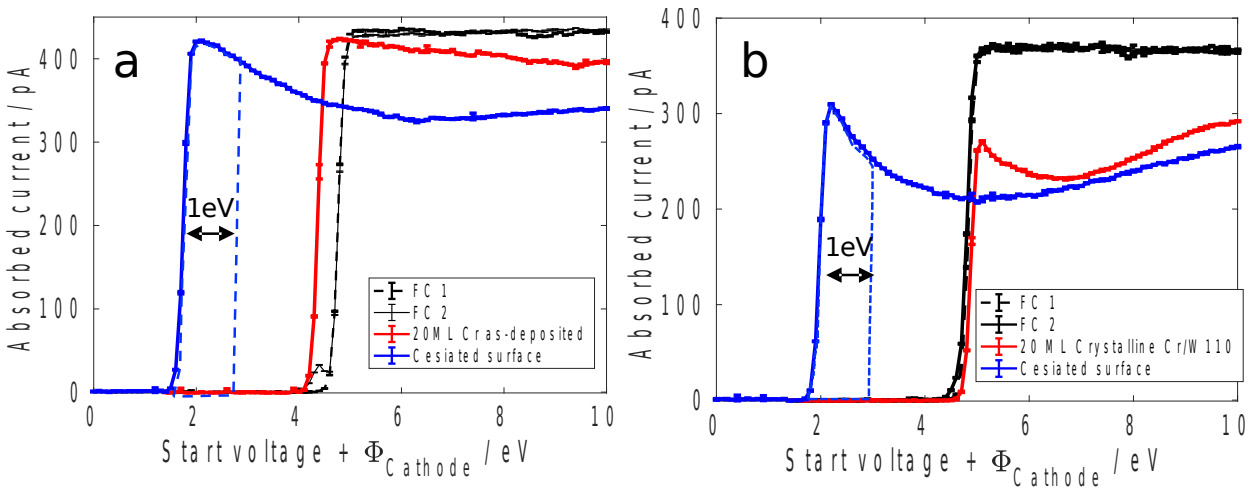

Fig. 3 – Absorbed current measurements on nano-crystalline Cr and on single crystalline Cr[110] surfaces. a) absorbed current on 20ML chromium film (red line), cesiated 20ML chromium (blue line) and total absorbed current (faraday cup measurements, black lines) labelled as FC1 (after Cr deposition) and FC2 (after cesiation of the surface). b) absorbed current on single-crystalline chromium [110] film (red line), cesiated chromium [110] (blue line) and total absorbed current (Faraday cup measurements, black lines) labelled as FC1 (after Cr crystallization) and FC2 (after cesiation of the Cr[110] surface). Blue shaded regions indicate the electron absorption in the energy-relevant range for TECs.

Power conversion efficiency is a key figure of merit for thermionic energy converters. Previous optimization efforts used prototype TEC cells. While such measurements reveal a cell's performance characteristics, the cell itself

remains essentially a “black box” and the physics that controls performance must be inferred. Our in-operando electron absorption measurements demonstrate the value of LEEM experiments in “breaking open the black box”: by testing half-cells in-operando, quantitative observation of electron reflectivity point to new routes for mitigating performance-limiting space-charge cloud formation by optimizing the low-energy electron reflectivity of anode materials. We think the implementation of nano-engineered anodes with high electron absorption will generate new insights to increasing the overall efficiency of TECs, opening-up new routes for integration of micro-gaps into thermionics devices (see supplementary note #5).

In conclusion, understanding electron reflectivity is key to designing new electron collector materials for next generation of thermionic energy converters. We have shown that using as-deposited films without long-range crystalline order reduces electron reflectivity and increases electron collection at low work function electrodes, and thus presents a strategy for mitigating space-charging and the associated performance degradation in TEC applications. Our study demonstrates that cesiated nano-crystalline Cr films increase electron absorption to 96% compared to just 79% in cesiated Cr[110] films, suggesting an economical and scalable path toward electron anti-reflective anodes based on thin metal coatings that is also compatible for integration into micro-gap based technologies.

Supplementary material

See supplementary material for the complete analysis of work function, auger electron spectroscopy, and total electron reflection.

Acknowledgements

All experiments were performed in the spin polarized LEEM at the National Center for Electron Microscopy, Molecular Foundry, Lawrence Berkeley National Laboratory. The information, data, or work presented herein was funded in part by the Advanced Research Projects Agency-Energy (ARPA-E), U.S. Department of Energy, under Award Number DE-AR0000664. The views and opinions of authors expressed herein do not necessarily state or reflect those of the United States Government or any agency thereof. Work at the Molecular Foundry was supported by the Office of Science, Office of Basic Energy Sciences, of the U.S. Department of Energy under Contract No. DE-AC02-05CH11231.

[1] D.B. Go, J.R. Haase, J. George, J. Mannhart, R. Wanke, A. Nojeh, and R. Nemanich, Front. Mech. Eng. **3**, 1 (2017).
[2] G.N. Hatsopoulos and E.P. Gyftopoulos, *Thermionic Energy Conversion Volume I: Processes and Devices* (The Massachusetts Institute of Technology, 1973).
[3] J.-H. Lee, I. Bargatin, N.A. Melosh, and R.T. Howe, Appl. Phys. Lett. **100**, 173904 (2012).
[4] I.T. Lim, S.A. Lambert, J.-L. Vay, and J.W. Schwede, Appl. Phys. Lett. **112**, 073906 (2018).
[5] M. Islam, O.T. Inal, and J.R. Luke, J. Appl. Phys. **100**, 084903 (2006).
[6] J.I. Flege, W.X. Tang, and M.S. Altman, *Characterization of Materials* (John Wiley & Sons, Inc., Hoboken, NJ, USA, 2002).
[7] E. Bauer, Reports Prog. Phys. **57**, 895 (1994).
[8] A.L.F. Cauduro, R. dos Reis, G. Chen, A.K. Schmid, H.-G. Rubahn, and M. Madsen, Ultramicroscopy **183**, 99 (2017).
[9] A.L. F. Cauduro, R. dos Reis, G. Chen, A.K. Schmid, C. Méthivier, H.-G. Rubahn, L. Bossard-Giannesini, H. Cruguel, N. Witkowski, and M. Madsen, ACS Appl. Mater. Interfaces **9**, 7717 (2017).
[10] Y. Murata, E. Starodub, B.B. Kappes, C. V. Ciobanu, N.C. Bartelt, K.F. McCarty, and S. Kodambaka, Appl. Phys. Lett. **97**, 143114 (2010).

[11] K.F. McCarty, J.C. Hamilton, Y. Sato, A. Saá, R. Stumpf, J.D. La Figuera, K. Thürmer, F. Jones, A. K Schmid, A.A. Talin, and N.C. Bartelt, New J. Phys. **11**, 043001 (2009).
[12] B. Santos, J.M. Puerta, J.I. Cerda, R. Stumpf, K. von Bergmann, R. Wiesendanger, M. Bode, K.F. McCarty, and J. de la Figuera, New J. Phys. **10**, 013005 (2008).
[13] E. Rotenberg, B.K. Freelon, H. Koh, A. Bostwick, K. Rossnagel, A. Schmid, and S.D. Kevan, New J. Phys. **7**, 114 (2005).
[14] A.G. Fedorus and A.G. Naumovets, Surf. Sci. **21**, 426 (1970).
[15] L. Camosi, S. Rohart, O. Fruchart, S. Pizzini, M. Belmeguenai, Y. Roussigné, A. Stashkevich, S.M. Cherif, L. Ranno, M. de Santis, and J. Vogel, Phys. Rev. B **95**, 214422 (2017).
[16] H.B. Michaelson, J. Appl. Phys. **48**, 4729 (1977).
[17] P.J. Berlowitz and N.D. Shinn, Surf. Sci. **209**, 345 (1989).
[18] *Various authors report the value of the work function of bulk cesium to be between 1.8eV and 2.2eV, and the small difference we see between cesium saturated nano-structured versus crystalline substrates may be the result of different crystallinity and orientation of the cesium layers.*
[19] N.S. Rasor and C. Warner, J. Appl. Phys. **35**, 2589 (1964).
[20] J.B. Taylor and I. Langmuir, Phys. Rev. **44**, 423 (1933).
[21] S.H. Chou, J. Voss, I. Bargatin, A. Vojvodic, R.T. Howe, and F. Abild-Pedersen, J. Phys. Condens. Matter **24**, 445007 (2012).
[22] E. Wimmer, A.J. Freeman, M. Weinert, H. Krakauer, J.R. Hiskes, and A.M. Karo, Phys. Rev. Lett. **48**, 1128 (1982).